ISPRS Journal of Photogrammetry and Remote Sensing A trunk-based SLAM backend for smartphones with online SLAM in large- scale forest inventories

Article *in* ISPRS Journal of Photogrammetry and Remote Sensing · April 2020

DOI: 10.1016/j.isprsjprs.2020.02.006

CITATION
1

READS
212

8 authors, including:

Tauheed Ullah Khan
Beijing Forestry University
20 PUBLICATIONS **54** CITATIONS
SEE PROFILE

Abdul Mannan
Beijing Forestry University
29 PUBLICATIONS **124** CITATIONS
SEE PROFILE

Sajjad Saeed
Beijing Forestry University
47 PUBLICATIONS **213** CITATIONS
SEE PROFILE

ISPRS Journal of Photogrammetry and Remote Sensing 162 (2020) 41–49

Contents lists available at ScienceDirect

ISPRS Journal of Photogrammetry and Remote Sensing

journal homepage: www.elsevier.com/locate/isprsjprs

A trunk-based SLAM backend for smartphones with online SLAM in large-scale forest inventories

Yongxiang Fan[a], Zhongke Feng[a,*], Chaoyong Shen[a], Tauheed Ullah Khan[b], Abdul Mannan[c], Xiang Gao[d], Panpan Chen[a], Sajjad Saeed[e]

[a] Precision Forestry Key Laboratory of Beijing, Beijing Forestry University, Beijing 100083, China
[b] School of Nature Conservation, Beijing Forestry University, Beijing 100083, China
[c] Forest, Wildlife and Fisheries Department, Government of Punjab, Lahore 54500, Pakistan
[d] School of Science, Anhui Agricultural University, Anhui 230036, China
[e] Department of Forestry & Wildlife Management, University of Haripur, Haripur22620, Pakistan

ARTICLE INFO

Keywords:
Forest inventory
Online SLAM
Smartphone
Augmented reality
Tree position
SLAM backend
Loop closure detection
Graph optimization

ABSTRACT

Reliable forest resource information is needed to assess the forest development status and design management plans for forest maintenance and conservation. The forest field sample inventory is a vital forest resource inventory method. Thus, forest inventory reliability depends on tree attribute estimation accuracy and the quantity and quality of field samples. Simultaneous localization and mapping (SLAM)-based mobile laser scanners (MLSs) are convenient inventory tools due to their mobility and global navigation satellite system (GNSS) signal independence. However, such scanners may be heavy, expensive and unable to verify results on-site. With the improved SLAM algorithm and chip computing capabilities, a smartphone can deploy an online SLAM system, which allows the smartphone to perform the relative positioning in forests without GNSS signals. Previous research studies have demonstrated this simple, portable, and economical device for estimating the tree position and diameter at breast height (DBH) through tree-by-tree measurements in real time. However, the device might face a challenge in large-scale forest inventories because the image-feature-based backend may not work well in forests that are not well constructed for traditional SLAM systems. In this paper, an online trunk-based backend was designed to accurately estimate tree position and correct pose drift in large-scale forest inventories in real time. Specifically, a trunk-based loop closure detection algorithm was designed for detecting whether an earlier observed tree is re-observed to provide nodes and constraints for tree position graph optimization; this algorithm uses the provided nodes and constraints to build and optimize the tree position graph and then correct the current pose based on the optimized globally consistent tree position graph. This new backend was integrated with the previous work as an executable program that can be deployed on a smartphone with an online RGB-D SLAM system. The method was tested in 5 field sample plots (32 × 32 m), and the reference tree positions were collected using terrestrial laser scanning (TLS) through multi-scan mode. The distance mean between the estimated and reference tree positions was 0.133 m when using our new backend, and it was 0.759 m when estimated with the RTAB-Map. The tree position estimates were unbiased and had root mean square errors (RMSEs) of less than 0.09 m in the x-axis, y-axis and z-axis directions when using the trunk-based backend. However, the estimates had biases of −0.125 m, −0.261 m and 0.262 m and RMSEs of more than 0.30 m in the x-axis, y-axis and z-axis directions without the new backend. The results showed that the designed trunk-based backend allows a smartphone with an online SLAM system to function as an accurate and efficient tool for large-scale forest inventories. However, the method was tested only in 32 × 32 m square field sample plots. More tests must be performed in larger plots in the future, although enough loop-closure constraints can theoretically guarantee the accuracy of the tree position graph and current pose.

* Corresponding author.
E-mail address: fengzhongke1@126.com (Z. Feng).

https://doi.org/10.1016/j.isprsjprs.2020.02.006
Received 28 June 2019; Received in revised form 10 February 2020; Accepted 10 February 2020

1. Introduction

Forests cover approximately one third of the Earth's land surface and play a vital role in climate regulation and the global carbon cycle; thus, they have attracted increasing interest from many researchers and policymakers (Köhl et al., 2015; Trumbore et al., 2015). Reliable forest resource information is needed for forest development status evaluation, such as climate change impact evaluations and carbon stock estimations, and forestry departments use it as the basis for creating forest development plans, such as forest cultivation and forest harvesting plans (Keenan et al., 2015; MacDicken, 2015). The forest field sample inventory is an important forest resource inventory method that provides forest area parameter data by summarizing the estimates obtained from all field samples in an area, which means that the reliability of forest inventories depends on the accuracy of field sample attribute estimates and the quality and quantity of the field samples (Liang et al., 2018a).

A forest field sample is usually a small representation of a forest area, normally with a circular shape with a radius of 4–15 m (Liang et al., 2016). The shape and area of a sample plot can vary according to the needs of the study. Traditionally, the tree attributes in the plot, such as species, diameter at breast height (DBH), tree height, and tree position, have been observed using simple tools, including callipers and clinometers, which have shown low efficiency and strong subjectivity. Moreover, it is hard to find a tool that can accurately estimate tree positions. However, these characteristics have changed dramatically since the emergence of light detection and ranging (LiDAR). In particular, terrestrial laser scanning (TLS), also known as a ground-based LiDAR, has been proven to be an accurate and efficient tool in small sample plots (Srinivasan et al., 2015; Liang et al., 2016; Liang et al., 2018).

The quality and quantity of the field samples are also important factors influencing forest inventory accuracy in large forest areas, and they can be improved by increasing the number and size of sample plots (Liang et al., 2018a). Practical considerations often limit the number of plots due to the complexity of the forest topography, especially in natural forests. Fortunately, the effects of numerical limitations can be counterbalanced by increasing the sample plot size. However, the inventories are also limited in terms of spatial coverage as efficient tools for providing sufficient and accurate data are lacking. TLS can also be used in large plots by collecting and merging different scans from multiple sites (Liang and Hyyppä, 2013; Pueschel et al., 2013).

In a large-scale forest inventory, devices with convenient measurement and efficient data acquisition methods are preferred. In recent years, one or more lasers were installed on a mobile platform to enable such a combined system, called a Mobile Laser Scanning (MLS) system, to efficiently collect data during movement. In terms of the speed of data collection, a previous study has proven that an MLS was several times faster than a TLS (Liang et al., 2015). A typical MLS system is an all-terrain vehicle (ATV) mounted with a global navigation satellite system (GNSS) receiver, an inertial measurement unit (IMU), and a laser scanner. The MLS can acquire the poses of the scanner by using the mounted sensors during movement in a forest, which means that the point sequence measured by the scanner can be transformed into the same reference coordinate and merged into a single point cloud based on the synchronized pose data (Qian et al., 2017; Bienert et al., 2018; Liang et al., 2018b). One challenge of the MLS is that the vehicle is difficult to manoeuvre in forests with complex ground conditions. However, the emergence of backpack and handheld MLSs has improved this situation (Ryding et al., 2015; Bauwens et al., 2016; Holmgren et al., 2017). Another challenge is that the poor GNSS signals under dense canopies make it difficult for the mobile scanning system to determine the location, even if a high-precision IMU is used. Simultaneous localization and mapping (SLAM) technology is one of the solutions that use the data sequence acquired during motion for estimating the relative poses in real time, and it is a vital solution for robot relative navigation (Bailey and Durrant-Whyte, 2006; Durrant-Whyte and Bailey, 2006). SLAM-aided and SLAM-based MLS have been used in forest inventories to obtain globally consistent point cloud data by evaluating and optimizing the internal consistency of measurements (e.g., image reprojection errors and distances between point clouds). The difference is that the former used SLAM technology to aid the GNSS + IMU positioning system for absolute positioning, while the latter used only a SLAM-based system for relative positioning (Tang et al., 2015; Pierzchała et al., 2018).

With the development of SLAM algorithms and the improvement of chip computing power, the SLAM system can be deployed on a smartphone with simple sensors such as cameras and IMUs (Marder-Eppstein, 2016; Hyyppä et al., 2018). The time of flight (ToF) camera, as an alternative to LiDAR, features low power consumption and small size, and it can be embedded in smartphones to capture dense point clouds (Foix et al., 2011). Tomaštík et al. (2017) evaluated the availability of dense point clouds acquired by a SLAM-based smartphone with a ToF camera in small forest sample plots. Fan et al. (2018) provided a solution for the real-time estimation of tree attributes such as DBH, height and tree position using a SLAM-based smartphone in tree-by-tree mode in small sample plots. This online SLAM solution used augmented reality (AR) technology to display the observed results on the smartphone screen in real time, which allows observers to evaluate the measurements in situ. Obviously, the online SLAM-based smartphones are user friendly, simple, economical and light compared to traditional MLSs. However, the accuracy of such a device in a complex and large-scale forest inventory requires further scientific assessment.

The graph-based SLAM algorithm is widely used in current SLAM systems, which consist of two parts: a frontend and a backend (Grisetti et al., 2010). The frontend is typically for feature-based visual odometry (VO) or visual inertial odometry (VIO), which is used to estimate poses in real time (Fraundorfer and Scaramuzza, 2011; Scaramuzza and Fraundorfer, 2012); the backend is an optimization mechanism that can correct the drifts generated during the frontend pose estimation process by appearance-based loop closure detection and pose graph optimization (Grisetti et al., 2010). For feature-based frontends and appearance-based loop closure detection, good features are guaranteed to accurately estimate the poses and build globally consistent maps that should have localization accuracy, repeatability and distinctiveness. However, in the same area, the observed corners and blobs, which are usually used as features in SLAM algorithms, may be completely different from different perspectives because forests are not well structured for typical SLAM systems, which might present a challenge for the SLAM systems, especially in large-scale or complex forests (Pierzchała et al., 2018). Therefore, the SLAM-based device may not accurately measure tree positions, which are directly linked to 3D forest structures.

Tree trunks have proven to be good features in forest inventories. Chen et al. (2016) merged scans from an MLS with tree trunks as features, which improved the positioning accuracy by approximately 50%. Similarly, Kukko et al. (2017) used tree trunks as pose graph optimization nodes to correct MLS scan poses, which increased the planar accuracy of the tree positions by at least 50%. Obviously, the graph-based SLAM system, which takes tree trunks as features, may improve the accuracy of pose and tree position estimates in large-scale and complex forests. In this paper, a trunk-based backend was designed for an online SLAM-based smartphone, and it made the smartphone capable of positioning and estimating tree positions with high accuracy in large-scale forest in situ inventories.

2. Pose graph problem

In this study, an online Red Green Blue Depth (RGB-D) SLAM-based forest inventory system was deployed on a smartphone (Lenovo Phab 2 Pro) to collect tree attribute information tree-by-tree (Fan et al., 2018). The graph-based SLAM system on the phone used a VIO as the frontend and real-time appearance-based mapping (RTAB-Map) as the backend

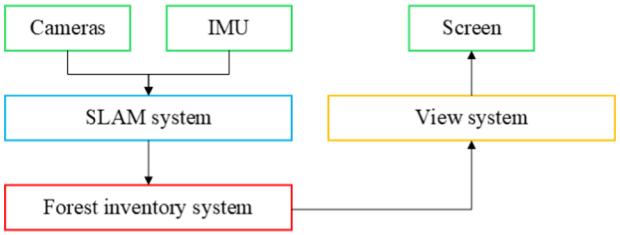

Fig. 1. The workflow of a typical smartphone-based forest inventory system.

(Labbé and Michaud, 2011; Labbé and Michaud, 2013; Labbé and Michaud, 2019) and provided pose, image and point cloud data in real time based on the mounted cameras and IMUs. The collected data was used to estimate tree attributes, including DBH and tree position. A typical smartphone-based forest inventory system structure is shown in Fig. 1. An AR scene was constructed to show the measured tree information, and it provided a detection result mechanism for observers through the smartphone screen (Fig. 2a).

The main problem with this feature-based SLAM system was that the pose estimation errors could not be corrected in forests, although the RTAB-Map, as the backend, could be used for online large-scale and long-term operation (Labbé and Michaud, 2013). The pose estimation error gradually accumulated and caused a large pose drift during the observation process, especially for large-scale sample plots. As an example, the position drift error exceeded 2 meters in a 1024-square-meter filed sample plot (Fig. 2b). Furthermore, the drift also led to inaccurately estimated tree positions (Fig. 3).

3. Materials and methods

3.1. Study area

The study area is located west of Beijing, China (N39°59′ E116°11′); it is primarily a managed forest but also includes some recreational and protected areas. Five square plots (32×32 m) were selected as sample plots for this study. Table 1 provides basic descriptions of the study sample plots.

3.2. The design of the trunk-based SLAM backend

In pose graph optimization, the poses are treated as nodes, and the observed transformations between poses are considered edges (or constraints) between nodes. Then, all the poses and constraints form a pose graph that can be optimized to correct the poses. In the optimization, loop constraints are constructed by revisiting the areas that have already been observed. Similarly, the tree position estimations in the field sample are regarded as nodes. The relative position differences between continuously observed trees are regarded as edges (or constraints) between nodes (Fig. 3). In addition, the loop constraints are constructed by re-observing the trees measured earlier. Then, all tree position estimations are corrected by optimizing the tree position graph, and the smartphone pose is corrected based on the resulting global consistent tree position graph. During the process, two important steps were completed: (1) loop closure detection for identifying earlier measured trees and (2) tree position graph optimization for optimizing all tree positions and correcting the smartphone pose based on the optimized tree position graph.

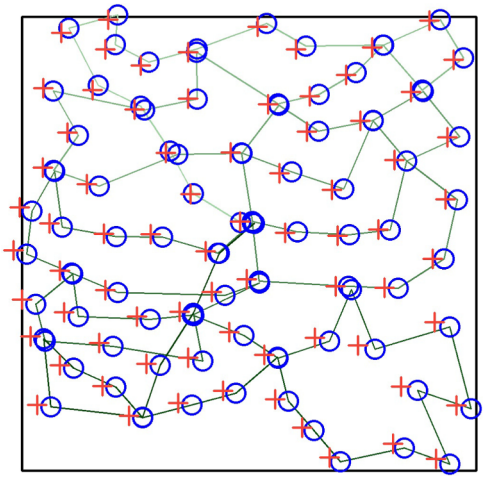

Fig. 3. The tree position estimates using the RTAB-Map as the backend of the SLAM system: the red plus signs indicate the stem references; the blue circles indicate the estimations, and the green lines indicate the observation order of the trees. (For interpretation of the references to colour in this figure legend, the reader is referred to the web version of this article.)

Table 1
Summary statistics of plot attributes.

Plot	Dominant Species	Stem Density (stems/ha)	DBH(cm)			
			Mean	SD	Min	Max
1	Ginkgo biloba	723	20.30	5.18	14.5	38.8
2	Fraxinus chinensis	732	18.13	2.35	12.4	25.6
3	Salix matsudana	537	21.67	5.27	13.1	35.0
4	Robinia pseudoacacia	762	19.46	4.61	10.3	37.3
5	Robinia pseudoacacia	703	18.63	3.65	11.2	28.4

3.2.1. The system structure

In this study, the traditional feature-based SLAM backend was not used in the forest inventory system; only the VIO system was used to estimate poses and obtain information such as tree positions and DBH based on the work by Fan et al. (2018) (Fig. 4). The loop closure detection provided new nodes and constraints for the tree position graph optimization by considering the tree position and DBH of the detected tree obtained by the inventory system as input. The tree position graph

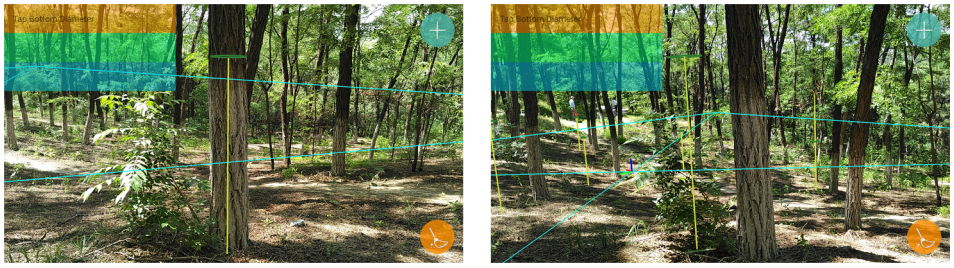

(a) (b)

Fig. 2. The AR scenes of observation: (a) the AR scene of a measurement just after observation; (b) the AR scene of the measurement after pose drift; the yellow lines indicate the breast heights and positions of the tree; the green circles indicate the tree DBHs; the blue lines indicate the sample area. (For interpretation of the references to colour in this figure legend, the reader is referred to the web version of this article.)

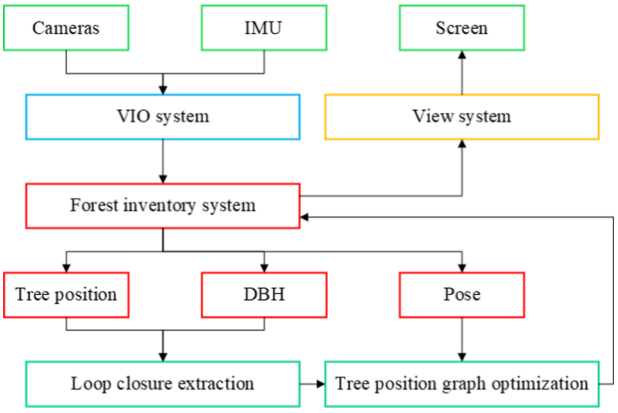

Fig. 4. The structure of the forest inventory system based on the trunk-based backend.

optimization method was used to build and optimize the tree position graph formed by all nodes and constraints and correct the current pose based on the optimized global consistent tree position graph. Then, the corrected pose was provided to the inventory system to adjust the AR scene.

3.2.2. Loop closure detection

The loop constraints are important tree position graph components; thus, some of the trees in a particular sample plot were observed multiple times during the observation process to construct this type of constraint. The task of the loop closure detection algorithm is to determine whether a newly measured tree is one of the earlier measured trees. We designed three features that can be constructed using tree positions and DBHs for the newly observed tree and one of the earlier observed trees to be tested to make this determination:

$$\mathbf{X} = \begin{bmatrix} x_1 \\ x_2 \\ x_3 \end{bmatrix} = \begin{bmatrix} d_t - d_0 \\ \|\mathbf{x}_t - \mathbf{x}_0\| \\ \frac{\|\mathbf{x}_t - \mathbf{x}_0\|}{\sum_{i=0}^{t-1} \|\mathbf{x}_{i+1} - \mathbf{x}_i\|} \end{bmatrix} \tag{1}$$

where $x_1$is the DBH error between the newly observed tree and the tested tree; $x_2$and $x_3$are the absolute distance and relative distance between the newly observed tree and the tested tree, respectively; d_0 and d_t are the DBH measurements of the newly observed tree and the tested tree; x_0 and x_t are their respective position measurements; and $\sum_{i=0}^{t-1} \|\mathbf{x}_{i+1} - \mathbf{x}_i\|$ represents the sum of the distance differences between continuously measured trees after the tested tree is observed. The three features were considered as Gauss distributions with a mean of zero based on the distribution characteristics of loop closure samples (Fig. 5), and they were normalized to ensure that they have the same variability:

$$\widetilde{\mathbf{X}} = \begin{bmatrix} \widetilde{x}_1 \\ \widetilde{x}_2 \\ \widetilde{x}_3 \end{bmatrix} = \begin{bmatrix} \frac{x_1}{\sqrt{2}\sigma_{DBH}} \\ \frac{x_2}{\sigma_2} \\ \frac{x_3}{\sigma_3} \end{bmatrix} \tag{2}$$

where σ_{DBH}, σ_2 and σ_3 are the standard deviations of the DBH, absolute distance error and relative distance error, respectively, which were estimated based on previously collected loop closure samples. Then, the model of logistic regression was designed as follows:

$$P(\widetilde{\mathbf{X}}) = \frac{1}{1 + e^{w_1\widetilde{x}_1^2 + w_2\widetilde{x}_2^2 + w_3\widetilde{x}_3^2 - 1}} \tag{3}$$

where w_1, w_2 and w_3 are the parameters, and they were determined to equal 9.861 and 0.03634 and 0.00008971, respectively, by fitting collected loop closure samples (Fig. 6).

The loop closure detection workflow was designed as shown in Fig. 7. When a tree was observed, the earlier measured trees that were less than 3 meters from this newly measured tree were selected as candidate trees for determining whether this newly measured tree was one of the already observed trees. Then, the normalized features of all candidate trees were calculated, and the probabilities of the candidate trees being re-observed were calculated using the logistic regression model. If the candidate tree with the highest probability had a probability greater than 0.5, then the tree was considered to be the same tree as the newly observed tree, and a loop constraint between the last observed tree and this candidate tree was provided for tree position graph optimization. Otherwise, a new tree position node and non-loop constraint between the new and last observed trees was provided.

3.2.3. Tree position graph optimization

Tree position graph optimization was used to optimize all tree position estimations and correct the current pose in real time. As shown in Fig. 8, after the new node and/or constraint were provided by the loop closure extraction, they were added to the tree position graph. The graph was optimized if the new constraint was a loop constraint. Then, the current pose was corrected based on the optimized tree position graph.

The tree position graph consists of nodes representing the tree positions and constraints between the nodes representing the positional changes between the continuously measured trees (Fig. 9). When optimizing the tree positions, all nodes are basically considered variables to be optimized. The purpose of tree position graph optimization is to minimize the differences between the constraints and the tree position changes by adjusting the tree position estimates.

When the graph was constructed, the tree position graph optimization problem was described as a cost function

$$F(\mathbf{x}) = \sum_{\langle i,j\rangle \in \zeta} e(\mathbf{x}_i, \mathbf{x}_j, \mathbf{z}_{ij})^T \Omega_{ij} e(\mathbf{x}_i, \mathbf{x}_j, \mathbf{z}_{ij}) \tag{4}$$

where $\mathbf{x}$ presents all tree positions, $\mathbf{x}_i$ and $\mathbf{x}_j$ are the tree positions of the ith and jth trees, respectively, $\mathbf{z}_{ij}$ and Ω_{ij} are the observed tree position coordinate difference and information matrix between the ith and jth trees, respectively, and ζ is a set indicating tree pairs observed by neighbours.

$$e(\mathbf{x}_i, \mathbf{x}_j, \mathbf{z}_{ij}) = \mathbf{x}_j - \mathbf{x}_i - \mathbf{z}_{ij} \tag{5}$$

is used to calculate the error between the expected tree position coordinate difference and the observed value between the ith and jth tree. Obviously, the cost function is a representation of the sum of all constraint errors; thus, the optimization problem was solved by minimizing this function:

$$\mathbf{x}^* = \underset{\mathbf{x}}{\operatorname{argmin}} F(\mathbf{x}) \tag{6}$$

$F(\mathbf{x})$ is a sparse function that can be solved directly using sparse Cholesky factorization. In addition, the information matrix Ω_{ij} was designed as a diagonal matrix formed by the vector $\mathbf{z}_{ij} = [x_1, x_2, x_3]^T$ in the optimization process:

$$\Omega_{ij} = \begin{bmatrix} |x_1| & 0 & 0 \\ 0 & |x_2| & 0 \\ 0 & 0 & |x_3| \end{bmatrix} \tag{7}$$

Fig. 10 shows the optimization result of the tree position graph mentioned in Fig. 3.

Once the tree position graph was optimized when a loop constraint was added, the current pose was corrected using the optimized tree position graph. Before optimization, a coordinate system (auxiliary tree position coordinate system, ATPCS) was established based on the newly observed tree. The origin of this coordinate was the position of the newly observed tree; the x-axis direction points horizontally to the position of the last measured tree, the z-axis points vertically upward,

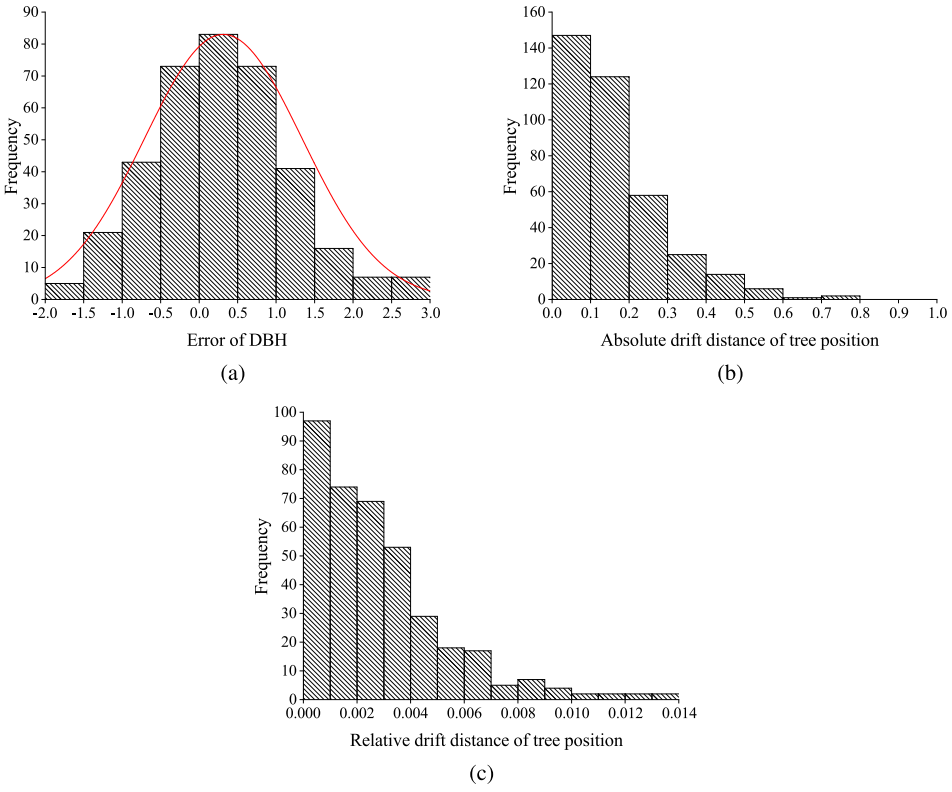

Fig. 5. The distribution characteristics of different feature samples: (a) the histogram of the DBH errors; (b) the histogram of the absolute tree position drift distance; (c) the histogram of the relative tree position drift distance.

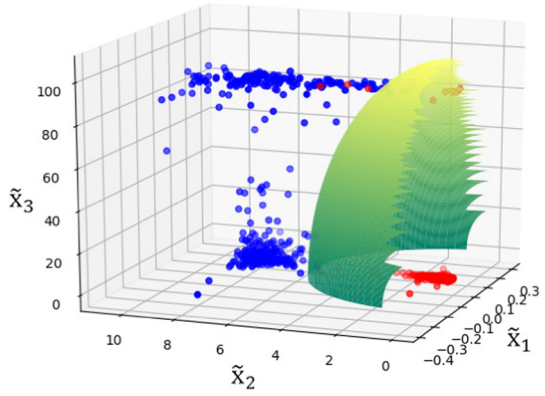

Fig. 6. The classification result of the logistic regression model; red points indicate positive samples; blue points indicate negative samples; the green surface indicates the model. (For interpretation of the references to colour in this figure legend, the reader is referred to the web version of this article.)

and the y-axis and the other two axes form this right-handed coordinate system. The current pose was described in the ATPCS. After optimization, the ATPCS was established based on the optimized tree positions. Therefore, the current pose described in the ATPCS was converted to the world coordinate system again, which was considered the corrected current pose

$$T'_w = T'_{wa} T_{aw} T_w \tag{8}$$

where T'_w was the corrected current pose; T'_{wa} is the transformation matrix from the ATPCS to the world coordinate system (WCS), which was determined after optimization; T_{aw} is the transformation matrix from the WCS to the ATPCS, which was determined before optimization; and the pose matrix T_w was the current pose before optimization. Fig. 11 shows the AR scenes before and after pose correction.

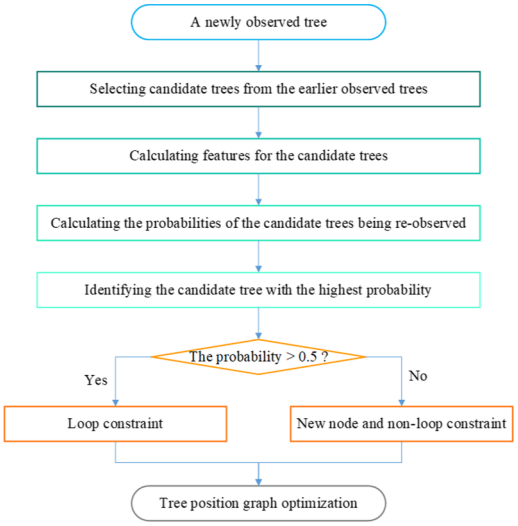

Fig. 7. The workflow of the trunk-based loop closure extraction.

3.3. Study methods

In this paper, the correction of the current pose mainly depended on the optimized tree position graph, and the corrected pose affected the optimization of the tree position graph thereafter. Therefore, the accuracy of the tree position was used to indirectly evaluate the pose accuracy, which is a major concern in forestry inventories. To accurately evaluate the tree position measurements, references were collected using a TLS (FARO Photon 120) through a multi-scan method (Fig. 12). During the scanning process, artificial spheres were set up as reference targets in the field samples to merge the acquired multi-scan data. The merged point clouds were processed using the method proposed by Cabo et al. (2018). The accuracy of the tree position was

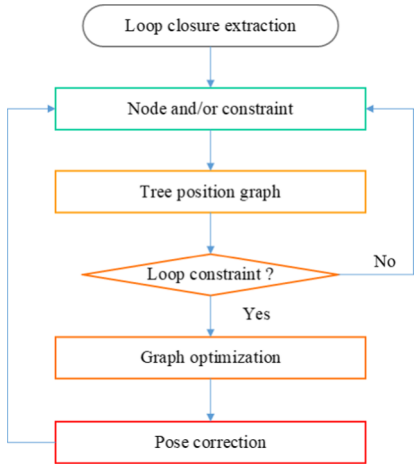

Fig. 8. The tree position graph optimization workflow.

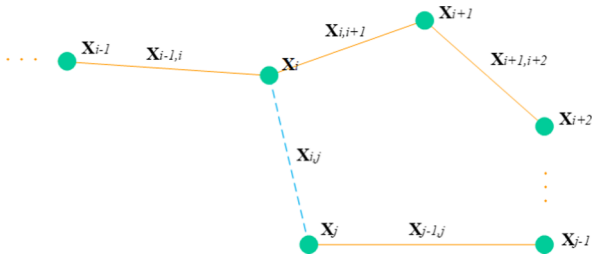

Fig. 9. The basis of the tree position graph: the green circles indicate nodes; the orange lines indicate non-loop constraints; the light blue line indicates a loop constraint. (For interpretation of the references to colour in this figure legend, the reader is referred to the web version of this article.)

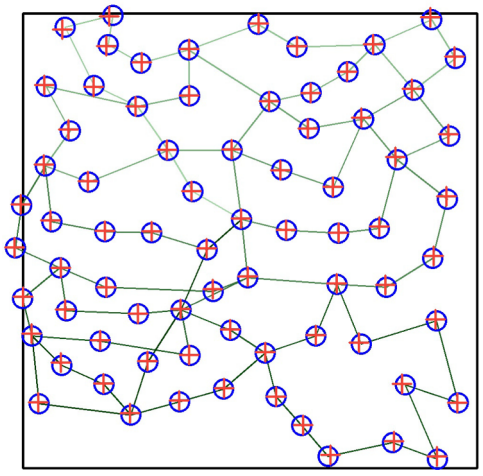

Fig. 10. A typical optimization result of the tree position graph mentioned in Fig. 3; the red plus signs indicate the stem references; the blue circles indicate the optimized tree positions; the green lines indicate the observation order of the trees. (For interpretation of the references to colour in this figure legend, the reader is referred to the web version of this article.)

evaluated using the mean distance, bias and root mean square error (RMSE), as defined in the following equations:

$$mean = \frac{\sum_{i=1}^{n} \|\mathbf{x}_i - \mathbf{x}_{ir}\|}{n} \quad (9)$$

$$bias = \frac{\sum_{i=1}^{n} (x_i - x_{ir})}{n} \quad (10)$$

$$RMSE = \sqrt{\frac{\sum_{i=1}^{n} (x_i - x_{ir})^2}{n}} \quad (11)$$

where $\mathbf{x}_i$ is the ith measurement of the tree position, $\mathbf{x}_{ir}$ is the ith reference, $n$is the number of estimates, x_i is a coordinate component of the ith tree position measurement in the direction of the x-axis, y-axis or z-axis, and x_{ir} is the corresponding reference with x_i. The mean distance indicates the mean drift distance of the tree position measurements, bias describes the difference between all estimates and references, and RMSE indicates the variability of all position errors.

4. Results

Our estimates showed that the mean of the distances between the tree position estimates and the references based on the RTAB-Map method (0.759 m) was five times that of our trunk-based backend method (0.133 m) (Table 2). The maximum distance estimated with the former method was more than 2.0 m, while it was considerably lower (0.32 m) in our method. Our comparative analysis showed that the distance between the estimated tree position and the reference gradually increased as the observation process progressed when using the RTAB-Map method, while it was less than 0.2 m and remained almost stable during the process using the trunk-based backend (Fig. 13).

The tree positions acquired based on the RTAB-Map backend showed a significant bias (Table 3) that exceeded 0.80 m in the x-axis direction in plot 1. However, the tree positions based on the trunk-based backend were unbiased, and the max bias was only −0.07 m in the z-axis direction in plot 1. Fig. 14 shows the scatter plots of the tree position estimate errors in all sample plots, which indicated that the biases of the estimates based on two different backends had different properties. The errors of the data acquired based on the optimized backend method are concentrated near the reference point, while the errors of the data obtained based on the RTAB-Map method are very far from the unbiased point and not evenly spread around the reference point (Fig. 14). The RMSEs of the tree position estimate obtained based on the RTAB-Map backend in all plots were significantly larger than those obtained by the optimized backend (Table 3, Fig. 14). The overall RMSEs based on the RTAB-Map method were greater (0.3 m) than that of our method, which was less than 0.09 m.

5. Discussion

The aim of this work was to design a trunk-based backend for optimizing the accuracy of the estimated tree positions and correcting the pose drift in real time based on the optimized tree position graph. Then, the designed system was deployed on a user-friendly smartphone with an online SLAM system that could be used in large-scale forest inventories with high precision and accuracy. The test results showed that the mean distance between the estimated and reference tree positions was 0.12 m. The tree position estimates were unbiased (−0.006 m, 0.001 m, 0.036 m in the x-axis, y-axis and z-axis directions) and had RMSEs of 0.085 m, 0.086 m and 0.078 m in the three axis directions.

Many previous studies have attempted to improve tree position estimate accuracy using different equipment and methods. Liang et al. (2018) evaluated the availability of an MLS that relies on GNSS + IMU positioning, in large-scale forest inventories under different stand conditions; their results showed RMSEs higher than 0.5 m under any stand conditions. Compared to the methods used in earlier studies, our results were higher mainly due to the occlusion of the GNSS signal in the forests. Tang et al. (2015) used a SLAM-aided positioning solution with point clouds collected by a small-footprint mobile LiDAR to improve the positioning accuracy of the GNSS + IMU system and reported a trajectory RMSE of 0.32 m in the horizontal direction, which was less accurate than our results. However, their test areas were larger than the sample fields in our paper; therefore, it is impossible to determine which method has higher precision. Pierzchała et al. (2018) used a

(a) (b)

Fig. 11. A typical sample of the AR scenes before and after pose correction: (a) the AR scene before pose correction; (b) the AR scene after pose correction; the yellow lines indicate the breast heights and positions of the tree; the green circles indicate the DBHs of the tree; the blue lines indicate the sample area. (For interpretation of the references to colour in this figure legend, the reader is referred to the web version of this article.)

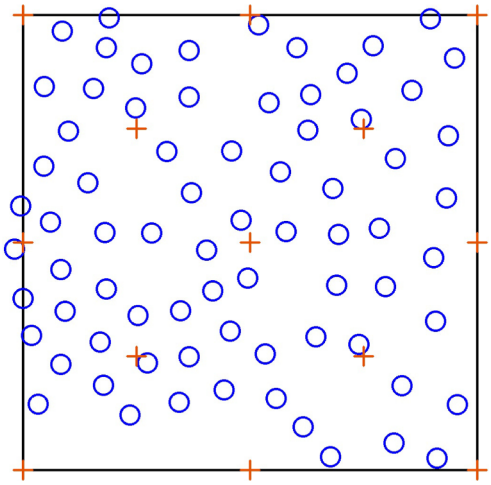

Fig. 12. The TLS scanning scenario; the black lines indicate sample field boundaries; the blue circles indicate tree positions; and the orange plus signs indicate the scanning locations. (For interpretation of the references to colour in this figure legend, the reader is referred to the web version of this article.)

Table 2
Statistical results of the distances between the tree position estimates and the references.

Plot	Mean Distance (m)		Max Distance (m)	
	RTAB-Map	Trunk-based Backend	RTAB-Map	Trunk-based Backend
1	0.922	0.148	1.36	0.28
2	0.981	0.137	2.07	0.30
3	0.615	0.124	1.25	0.26
4	0.530	0.142	1.64	0.23
5	0.717	0.112	1.16	0.32
Total	0.759	0.133	2.07	0.32

stereo SLAM system to improve the positioning accuracy of the GNSS + IMU system. Their results showed that the mean error of the relative distance estimation between trees was 0.0476 m but that there were four outliers. The accuracy of this study was higher than ours, but our results did not contain any outliers.

Most current SLAM systems work based on features such as corners and blobs. A good feature will help improve the positioning accuracy of the SLAM system. A good feature should have localization accuracy, repeatability, robustness and invariance. However, it is difficult to find good features, especially in forests with complex vegetation. Chen et al. (2016) used the tree position and DBH information contained in a single scan to match scans and obtain globally consistent point clouds that can be used to extract tree information. Their results showed a mean error of 2.33 m, which was 50% better than the results for which the scan matching procedure was not carried out; however, their accuracy was still lower than ours. Kukko et al. (2017) added constraints between tree stem locations in the graph optimization to correct the poses of the scans, which were then used to merge different scans; their results showed mean distances of 0.070 0.46 m and standard deviations of 0.005 0.008 m between the optimized and reference tree positions, and these results were better than ours.

The ToF camera, which was used as a replacement for LiDAR, features low power consumption and a small size, and thus, it can be embedded in a smartphone to build an RGB-D SLAM system, which allows the phone to be used for relative positioning and point cloud acquisition for the surrounding environment independent of GNSS signals. Tomaštík et al. (2017) scanned sample fields with a smartphone with an online RGB-D SLAM system, and the results extracted from the scan point clouds showed a RMSE of 0.2 m for the better scanning pattern, which was less accurate than our results. In addition, this scanning device was less efficient than the laser scanner due to the limited measurement distance of the ToF camera. Fan et al. (2018) enabled a smartphone with an online RGB-D SLAM system to observe tree positions, DBH and tree height tree-by-tree in real time. In their tests, the plot grounds were mapped before observing the trees to reduce pose drift during of observation, and their results showed a RMSE of 0.12 m in both the x-axis and y-axis directions, which was similar to our results. However, the sample plots they used were much smaller than those we used in this study.

Although the newly designed SLAM backend enables mobile phones with SLAM systems to be used in large-scale forest inventories, it still faces some limitations. For example, (1) our method requires access to the trees that need to be observed tree-by-tree; thus, so it could be less efficient than LiDAR-based MLS methods; (2) it is also challenging for ground-based imagery to produce reliable and complete tree height information due to canopy occlusion, especially in mature forests; (3) in trunk-based loop closure detection, it must be accurately determined whether a newly measured tree is one of the trees that has been observed; however, the probability model we constructed could make some errors, although this did not occur during this study; (4) this paper used only the methods of detecting the DBH height from the ground and estimating the horizontal position of trees described in Fan et al. (2018), which may affect the optimization result of our backend; and (5) our backend was tested based on the work of Fan et al. (2018), who used the RGB-D SLAM system implemented by Google Tango technology, which has been terminated, to estimate the tree properties. Unfortunately, these problems were encountered, but some of them will be addressed in the future. For example, (1) as the amount of experimental data increases, the probability model of loop closure detection could gradually improve; (2) some new monocular SLAM systems for mobile phones have been released, such as ARKit (Buerli and Misslinger, 2017) and ARCore (Lanham, 2018), and it is believed that forest inventory systems based on these technologies will be implemented in the future; and (3) some other light, low-cost alternatives, such as a Backpack-Mounted Omnidirectional Camera with Off-the-Shelf Navigation Sensors (Campos et al., 2018), have been developed and efficiently used in forest inventories.

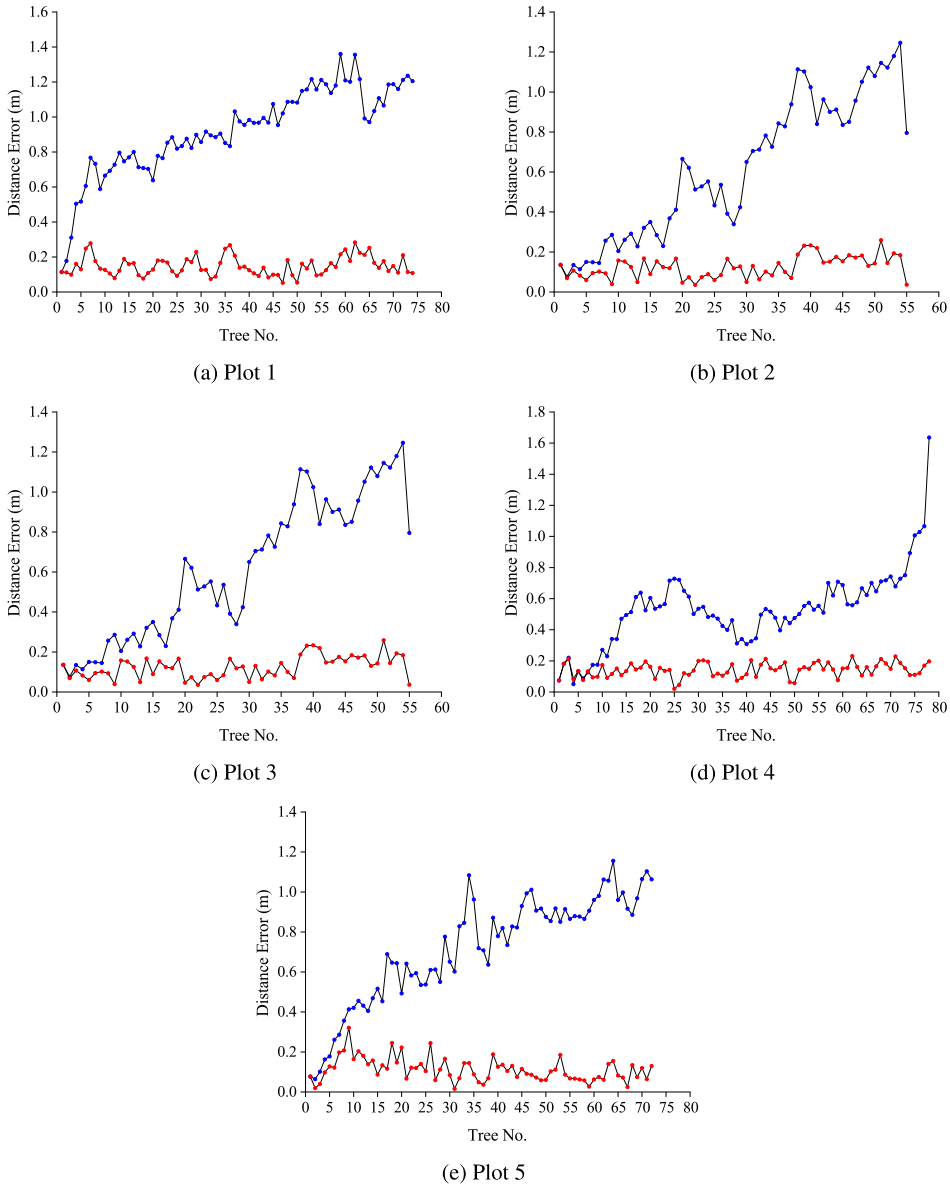

Fig. 13. Distance between the observed and reference tree positions during observation; blue points indicate the distance based on the RTAB-Map backend; red points indicate the distance based on the trunk-based backend. (For interpretation of the references to colour in this figure legend, the reader is referred to the web version of this article.)

Table 3
Accuracy of the tree position estimates based on the RTAB-Map backend and the trunk-based backend.

Plot	Bias (m)						RMSE (m)					
	RTAB-Map			Trunk-based Backend			RTAB-Map			Trunk-based Backend		
	x	y	z	x	y	z	x	y	z	x	y	z
1	0.818	0.072	0.323	0.048	0.069	−0.077	0.842	0.198	0.403	0.087	0.097	0.089
2	−0.510	−0.708	0.327	−0.044	−0.037	−0.013	0.601	0.868	0.367	0.101	0.099	0.051
3	−0.534	−0.138	0.146	−0.002	−0.008	−0.061	0.639	0.246	0.172	0.061	0.059	0.105
4	0.049	−0.467	0.133	−0.028	0.001	−0.032	0.163	0.530	0.179	0.100	0.076	0.080
5	−0.571	−0.010	0.358	−0.003	−0.022	−0.004	0.622	0.222	0.388	0.062	0.089	0.064
Total	−0.125	−0.261	0.261	−0.006	0.001	−0.036	0.610	0.498	0.323	0.085	0.086	0.078

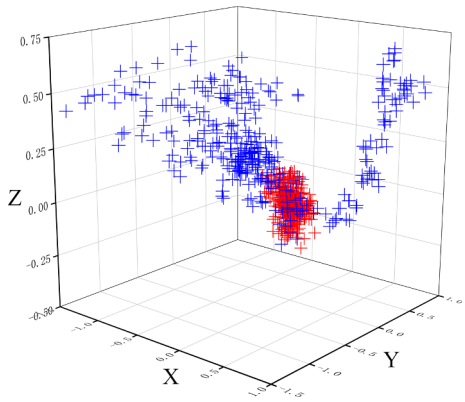

Fig. 14. Scatter plots of tree position errors in all plots; blue crosses indicate the position errors based on the RTAB-Map backend; red crosses indicate the position errors based on our backend. (For interpretation of the references to colour in this figure legend, the reader is referred to the web version of this article.)

6. Conclusion

In this study, we designed a trunk-based SLAM backend that includes two steps: trunk-based loop closure detection and tree position graph optimization. This backend was designed to assist in using a smartphone with an online SLAM system for large-scale forest inventories. This backend works based on recognizing trees that were previously observed. After integrating the backend with the method of estimating tree properties based on a smartphone with an RGB-D SLAM system, the new backend was tested in five 32 × 32 m square field samples. The results showed that the new backend can effectively improve tree position estimation accuracy in large-scale forest inventories. In addition, the improved AR scene with the corrected pose helped the observers determine whether a tree was previously observed.

In the future, the backend should be tested under complex forest conditions, such as areas with more shrubs, different tree species and forests of different ages, and the new test data should be used to improve the probability model in trunk-based loop closure detection. In addition, an observation trajectory should be designed, because it affects the loop closure node positions and thus affects the accuracy of the optimized tree positions and the current pose.

Acknowledgements

The authors are very thankful to the Fundamental Research Funds for the Central Universities (NO. 2015ZCQ-LX-01) and the National Natural Science Foundation of China (Grant No. U1710123) for funding and supporting this study.

References

Bailey, T., Durrant-Whyte, H., 2006. Simultaneous localization and mapping (SLAM): Part II. IEEE Robot. Autom. Magaz. 13 (3), 108–117.
Bauwens, S., Bartholomeus, H., Calders, K., Lejeune, P., 2016. Forest inventory with terrestrial LiDAR: a comparison of static and hand-held mobile laser scanning. Forests 7 (6), 127.
Bienert, A., Georgi, L., Kunz, M., Maas, H.G., von Oheimb, G., 2018. Comparison and combination of mobile and terrestrial laser scanning for natural forest inventories. Forests 9 (7), 395.
Buerli, M., Misslinger, S., 2017. Introducing ARKit-augmented reality for iOS. In: Apple Worldwide Developers Conference (WWDC 2017), pp. 1–187.
Cabo, C., Ordóñez, C., López-Sánchez, C.A., Armesto, J., 2018. Automatic dendrometry: tree detection, tree height and diameter estimation using terrestrial laser scanning. Int. J. Appl. Earth Observ. Geoinform. 69, 164–174.
Campos, M., Tommaselli, A., Honkavaara, E., Prol, F., Kaartinen, H., El Issaoui, A., Hakala, T., 2018. A backpack-mounted omnidirectional camera with off-the-shelf navigation sensors for mobile terrestrial mapping: development and forest application. Sensors 18 (3), 827.
Chen, Y., Tang, J., Khoramshahi, E., Hakala, T., Kaartinen, H., Jaakkola, A., Chen, R., 2016. Scan matching technology for forest navigation with map information. In: 2016 IEEE/ION Position, Location and Navigation Symposium (PLANS). IEEE, pp. 198–203.
Durrant-Whyte, H., Bailey, T., 2006. Simultaneous localization and mapping: part I. IEEE Robot. Autom. Magaz. 13 (2), 99–110.
Fan, Y., Feng, Z., Mannan, A., Khan, T., Shen, C., Saeed, S., 2018. Estimating tree position, diameter at breast height, and tree height in real-time using a mobile phone with RGB-D SLAM. Remote Sens. 10 (11), 1845.
Foix, S., Alenya, G., Torras, C., 2011. Lock-in time-of-flight (ToF) cameras: a survey. IEEE Sens. J. 11, 1917–1926.
Fraundorfer, F., Scaramuzza, D., 2011. Visual odometry: Part I: the first 30 years and fundamentals. IEEE Robot. Autom. Mag. 18 (4), 78–90.
Grisetti, G., Kummerle, R., Stachniss, C., Burgard, W., 2010. A tutorial on graph-based SLAM. IEEE Intell. Transp. Syst. Mag. 2, 31–43.
Holmgren, J., Tulldahl, H.M., Nordlöf, J., Nyström, M., Olofsson, K., Rydell, J., Willén, E., 2017. Estimation of tree position and stem diameter using simultaneous localization and mapping with data from a backpack-mounted laser scanner. Int. Arch. Photogram., Remote Sens. Spatial Inform. Sci. 42.
Hyyppä, J., Virtanen, J.P., Jaakkola, A., Yu, X., Hyyppä, H., Liang, X., 2018. Feasibility of Google Tango and Kinect for crowdsourcing forestry information. Forests 9 (1), 6.
Keenan, R.J., Reams, G.A., Achard, F., de Freitas, J.V., Grainger, A., Lindquist, E., 2015. Dynamics of global forest area: Results from the FAO global forest resources assessment 2015. For. Ecol. Manage. 352, 9–20.
Köhl, M., Lasco, R., Cifuentes, M., Jonsson, Ö., Korhonen, K.T., Mundhenk, P., Stinson, G., 2015. Changes in forest production, biomass and carbon: Results from the 2015 UN FAO Global Forest Resource Assessment. For. Ecol. Manage. 352, 21–34.
Kukko, A., Kaijaluoto, R., Kaartinen, H., Lehtola, V.V., Jaakkola, A., Hyyppä, J., 2017. Graph SLAM correction for single scanner MLS forest data under boreal forest canopy. ISPRS J. Photogram. Remote Sens. 132, 199–209.
Labbé, M., Michaud, F., 2011. Memory management for real-time appearance based loop closure detection. In: 2011 IEEE/RSJ International Conference on Intelligent Robots and Systems, IEEE, pp. 1271–1276.
Labbé, M., Michaud, F., 2013. Appearance-based loop closure detection for online large-scale and long-term operation. IEEE Trans. Rob. 29, 734–745.
Labbé, M., Michaud, F., 2019. RTAB-Map as an open-source lidar and visual simultaneous localization and mapping library for large-scale and long-term online operation. J. Field Robot. 36, 416–446.
Lanham, M., 2018. Learn ARCore-Fundamentals of Google ARCore: Learn to build augmented reality apps for Android, Unity, and the web with Google ARCore 1.0. Packt Publishing Ltd.
Liang, X., Hyyppä, J., 2013. Automatic stem mapping by merging several terrestrial laser scans at the feature and decision levels. Sensors 13, 1614–1634.
Liang, X., Wang, Y., Jaakkola, A., Kukko, A., Kaartinen, H., Hyyppä, J., Liu, J., 2015. Forest data collection using terrestrial image-based point clouds from a handheld camera compared to terrestrial and personal laser scanning. IEEE Trans. Geosci. Remote Sens. 53 (9), 5117–5132.
Liang, X., Kankare, V., Hyyppä, J., Wang, Y., Kukko, A., Haggrén, H., Holopainen, M., 2016. Terrestrial laser scanning in forest inventories. ISPRS J. Photogram. Remote Sens. 115, 63–77.
Liang, X., Hyyppä, J., Kaartinen, H., Lehtomäki, M., Pyörälä, J., Pfeifer, N., Huang, H., 2018a. International benchmarking of terrestrial laser scanning approaches for forest inventories. ISPRS J. Photogram. Remote Sens. 144, 137–179.
Liang, X., Kukko, A., Hyyppä, J., Lehtomäki, M., Pyörälä, J., Yu, X., Wang, Y., 2018b. In-situ measurements from mobile platforms: an emerging approach to address the old challenges associated with forest inventories. ISPRS J. Photogram. Remote Sens. 143, 97–107.
MacDicken, K.G., 2015. Global forest resources assessment 2015: what, why and how? For. Ecol. Manage. 352, 3–8.
Marder-Eppstein, E., 2016. Project tango. In: ACM SIGGRAPH 2016 Real-450 Time Live!, ACM. p. 40.
Pierzchała, M., Giguère, P., Astrup, R., 2018. Mapping forests using an unmanned ground vehicle with 3D LiDAR and graph-SLAM. Comput. Electron. Agric. 145, 217–225.
Pueschel, P., Newnham, G., Rock, G., Udelhoven, T., Werner, W., Hill, J., 2013. The influence of scan mode and circle fitting on tree stem detection, stem diameter and volume extraction from terrestrial laser scans. ISPRS J. Photogram. Remote Sens. 77, 44–56.
Qian, C., Liu, H., Tang, J., Chen, Y., Kaartinen, H., Kukko, A., Hyyppä, J., 2017. An integrated GNSS/INS/LiDAR-SLAM positioning method for highly accurate forest stem mapping. Remote Sens. 9, 3.
Ryding, J., Williams, E., Smith, M., Eichhorn, M., 2015. Assessing handheld mobile laser scanners for forest surveys. Remote Sens. 7, 1095–1111.
Scaramuzza, D., Fraundorfer, F., 2012. Visual odometry part II: matching, robustness, optimization, and applications. IEEE Robot. Autom. Magaz. 19 (2), 78–90.
Srinivasan, S., Popescu, S., Eriksson, M., Sheridan, R., Ku, N.W., 2015. Terrestrial laser scanning as an effective tool to retrieve tree level height, crown width, and stem diameter. Remote Sens. 7, 1877–1896.
Tang, J., Chen, Y., Hyyppä, J., Jaakkola, A., Kaartinen, H., Kukko, A., Holopainen, M., 2015. SLAM-Aided Stem Mapping for Forest Inventory with Small-Footprint Mobile LiDAR. Forests 6, 4588–4606.
Tomaštík, J., Saloň, Š., Tunák, D., Chudý, F., Kardoš, M., 2017. Tango in forests - an initial experience of the use of the new Google technology in connection with forest inventory tasks. Comput. Electron. Agric. 141, 109–117.
Trumbore, S., Brando, P., Hartmann, H., 2015. Forest health and global change. Science 349, 814–818.